

QArtSR: Quantization via Reverse-Module and Timestep-Retraining in One-Step Diffusion based Image Super-Resolution

Libo Zhu^{1*}, Haotong Qin^{2*}, Kaicheng Yang¹, Wenbo Li⁴,

Yong Guo⁵, Yulun Zhang^{1†}, Susanto Rahardja³, Xiaokang Yang¹

¹Shanghai Jiao Tong University, ²ETH Zürich, ³Singapore Institute of Technology,

⁴Chinese University of Hong Kong, ⁵Max Planck Institute for Informatics

Abstract

One-step diffusion-based image super-resolution (OSDSR) models are showing increasingly superior performance nowadays. However, although their denoising steps are reduced to one and they can be quantized to 8-bit to reduce the costs further, there is still significant potential for OSDSR to quantize to lower bits. To explore more possibilities of quantized OSDSR, we propose an efficient method, **Quantization via a reverse-module and timestep-retraining** for OSDSR, named **QArtSR**. Firstly, we investigate the influence of timestep value on the performance of quantized models. Then, we propose **Timestep Retraining Quantization (TRQ)** and **Reversed Per-module Quantization (RPQ)** strategies to calibrate the quantized model. Meanwhile, we adopt the module and image losses to update all quantized modules. We only update the parameters in quantization finetuning components, excluding the original weights. To ensure that all modules are fully finetuned, we add extended end-to-end training after per-module stage. Our 4-bit and 2-bit quantization experimental results indicate that QArtSR obtains superior effects against the recent leading comparison methods. The performance of 4-bit QArtSR is close to the full-precision one. Our code will be released at <https://github.com/libozhu03/QArtSR>.

1. Introduction

Image super-resolution (SR) aims to reconstruct high-resolution (HR) images from low-resolution (LR) inputs by recovering fine details. Recent diffusion-based SR methods [29, 42, 48] can capture intricate data distributions and produce HR images with exceptional perceptual quality by modeling high-dimensional structures more effectively. They perform better than numerous earlier traditional methods [5, 7, 10, 58], which focus on simple synthetic degradations (e.g., Bicubic downsampling). And GAN-based approaches [28, 43, 54] often suffer from training instability and performance fluctuations in real-world scenarios.

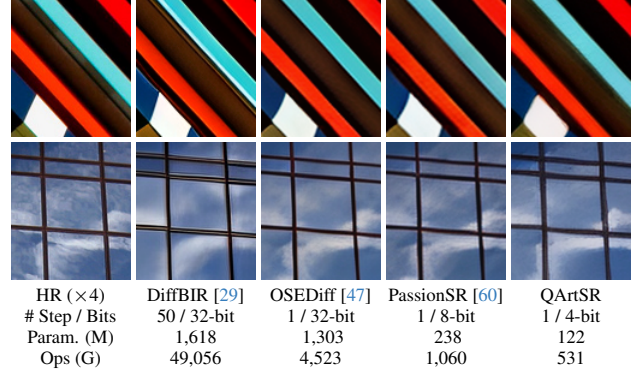


Figure 1. Visual results of full-precision (FP) and low-bit multi-step and/or one-step diffusion SR models. Ops are computed with output size 512×512 . Compared to FP OSEDiff, QArtSR achieves about 90.66% params reduction and $8 \times$ speedup.

While diffusion-based models achieve high-quality results, they come with high latency, computational costs, and storage demands, limiting the deployment of hardware devices. Researchers have explored various lightweight strategies, particularly reducing denoising steps. Fast samplers [37, 59] and distillation [38] significantly lower these steps. With advance of score distillation [46, 51], one-step diffusion SR (OSDSR) models, like SinSR [44], OSEDiff [47], and DFOSD [22], have become feasible.

To further compress OSDSR models, model quantization [9, 16, 21] stands out as an effective approach. Reducing activations and weights from full-precision (FP) to low-bit precision significantly decreases computational and storage costs. It is valuable under resource-constrained conditions. However, the inherent performance gap remains, necessitating strategies to minimize it for effective application in OSDSR models. PassionSR [60] is the first to introduce quantization to OSDSR, achieving 8-bit and 6-bit quantization. While 8-bit version maintains performance close to its FP counterpart (see Fig. 1), the reconstruction quality degrades sharply at 4-bit or lower precision (see Fig. 2). The ultra-low-bit quantization on both weights and activations has remained a challenging issue over time. It is hard for the ultra-low-bit quantized model to retain the performance.

*Equal contribution.

†Corresponding author: Yulun Zhang

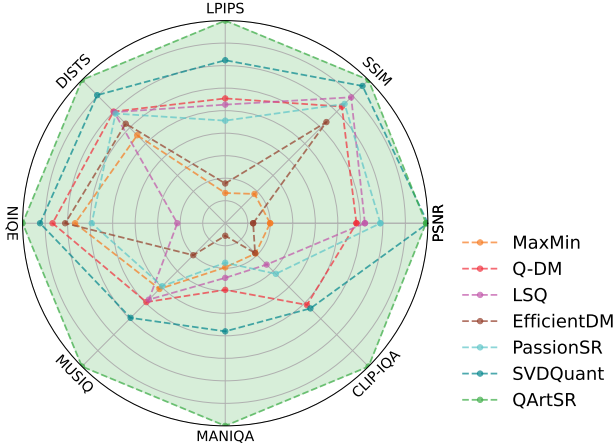


Figure 2. Performance visualization of low-bit quantization OSDSR methods at W4A4 bits setting on Urban100 [15].

Aiming at compressing the OSDSR further, we concentrate on addressing model quantization for ultra-low-bit settings. For multi-step diffusion’s ultra-low-bit quantization, current leading quantization strategies [14, 23, 27] have achieved promising results at 4-bit. However, applying these methods to OSDSR models still leads to substantial performance degradation (see Fig. 2). To improve model performance, we must address the following challenges:

I. Extremely constrained expression capability in low-bit settings. Under ultra-low-bit settings, quantized models exhibit significantly weaker expression capability than the full-precision one. The higher low-bit settings (*e.g.*, 8-bit) allow performance recovery through distillation with the full-precision counterpart. However, ultra-low-bit settings (*e.g.*, 2~4-bit) struggle to generate high-quality images or even complete image generation tasks. Due to the inherent performance ceiling of quantized models, distillation or similar methods bring limited improvement.

II. Severe optimization difficulties in discrete space. Converting a full-precision model to its quantized counterpart involves transitions from a continuous to a discrete space. In ultra-low-bit settings, the initial state in the discrete space is significantly distant from the optimal solution. Moreover, inaccurate gradients and quantization errors further hinder convergence, making it challenging for the quantized model to narrow its performance drop. As a result, achieving satisfactory performance demands extensive training time and computational resources.

III. Degradation of quantization for one-step features. According to our quantization experiments, many quantization methods present outstanding performance on multi-step diffusion models while weak performance on one-step diffusion models. This means that the quantization of the one-step diffusion model is quite different from the previous diffusion quantization work. We need to fully analyze the theoretical reason behind this phenomenon to design a more suitable quantization method for OSDSR.

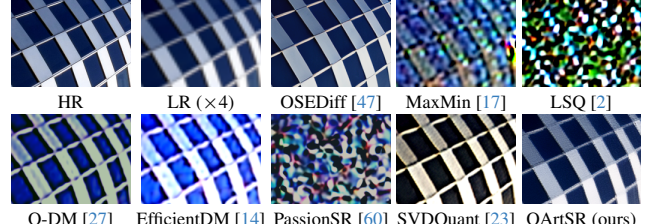


Figure 3. Visual comparison ($\times 4$) of 32-bit OSEDiff [47] and 2-bit quantized models with various quantization methods.

To alleviate those challenges, we propose an effective and efficient quantization method, **quantization via reverse-module and timestep-retraining** for one-step diffusion-based image super-resolution, named QArtSR.

We first explore the impact of timestep value on OSDSR quantization and propose the timestep retraining quantization (TRQ). It provides a better initial state for the quantized model, reducing the pressure of following the quantization process. Additionally, we propose a novel reversed per-module quantization (RPQ) strategy, whose quantization order is reversed to the inference sequence. By gradually introducing quantized modules, performance degradation can be recovered more effectively. The reversed order makes joint optimization of the image and module losses possible. We further apply extended training after the per-module stage, ensuring all modules are fully finetuned.

In the quantization process of our QArtSR, only the parameters in the specially designed finetuning components are updated with the combined loss, excluding the original weights. It is as efficient as recent post-training quantization methods, consuming similar GPU memory and time.

OSEDiff [47] is selected as our quantization foundation owing to its superior performance and high inference speed in QArtSR. Compared to 32-bit full-precision version OSEDiff [47], QArtSR achieves an impressive **90~95%** reduction in parameters and operations with 4~2 bits. In Figs. 1 and 3, QArtSR maintains perceptual quality comparable to full-precision models at 4-bit and preserves most performance even at 2-bit. Figure 2 demonstrates its superiority over state-of-the-art diffusion quantization methods. Overall, our key contributions are as follows:

- We propose an efficient ultra-low-bit quantization method for OSDSR, QArtSR. To the best of our knowledge, we are the first to quantize the OSDSR model to 2~4 bits on both the activation and weight efficiently.
- We propose a timestep retraining quantization (TRQ). We retrain the backbone with the best value of timestep, reducing the quantization error significantly.
- We propose a reversed per-module quantization (RPQ), considering the partial and overall losses meanwhile. The quantization order is reversed to the inference sequence.
- Our QArtSR delivers perceptual quality nearly matching that of a full-precision model at 4-bit. It significantly outperforms other leading quantization methods in both performance and scores across 2~4-bit settings.

2. Related Work

2.1. Image Super-Resolution

Reconstructing high-resolution (HR) images from low-resolution (LR) inputs degraded by complex factors has long been a challenging task, forming the core objective of image super-resolution (SR). Early SR techniques [6, 20, 57] and GAN-based approaches [28, 43, 54] have significantly advanced the field. Recently, stable diffusion (SD) models [34] have emerged as powerful tools, leveraging strong generative priors and the ability to model the intricate data distributions. Notable works, such as DiffBIR [29], SeeSR [48], and InvSR [53], have further improved perceptual quality. However, due to their multi-step nature, substantial inference latency is introduced, limiting real-world applications. To overcome this, one-step diffusion SR (OS-DSR) models (*e.g.*, SinSR [44], OSEDiff [47]) have been proposed, significantly reducing the inference time by condensing the process into a single step.

2.2. Model Quantization

Model quantization enhances performance by reducing parameter precision while preserving effectiveness. Depending on whether weight retraining is involved, quantization methods are categorized into post-training quantization (PTQ) [25, 50] and quantization-aware training (QAT) [2, 4, 52]. However, the distinction between PTQ and QAT has become increasingly blurred with the introduction of minor finetuning in PTQ. Quantization has also been demonstrated as an effective compression technique for deploying large language models [3, 26, 31, 32, 36] on terminal devices.

2.3. Quantization of Diffusion Models

With the rapid advances of diffusion models (DM), researchers have increasingly focused on improving their efficiency through quantization. PTQ4DM [35] pioneers the study of quantized diffusion models, identifying key challenges. Subsequent PTQ methods, such as Q-Diffusion [24] and PTQD [13], introduce specialized calibration strategies for diffusion models. Additionally, Q-DM [27] presents the first QAT-based method for low-bit multi-step DM, further advancing quantized diffusion. BitsFusion [39] and Bit-Distiller [11] have made significant progress in exploring weight-only quantization. The feedforward layer is recognized as particularly sensitive to quantization and model performance can be improved by selectively retraining it in QuEST [40]. Recently, EfficientDM [14] designs a low-rank quantization finetuning strategy and SVDQuant [23] utilizes 16-bit parallel low-rank skip-connection to retain the performance for multi-step DMs. As for one-step diffusion-based SR (OSDSR) models, PassionSR [60] proposes a novel quantization strategy and first quantizes OSDSR to 8-bit and 6-bit. However, limited research has focused on the ultra-low-bit (*i.e.*, 2~4-bit) quantization of OSDSR, which differs considerably from multi-step DM.

3. Methods

3.1. Preliminaries

Diffusion Models. Diffusion models [34] iteratively transform a complex data distribution into a simpler one by gradually adding noise. The reversed process, which reconstructs the data, is learned to generate new samples. The true data distribution is denoted as $p_{\text{data}}(\mathbf{x})$. The forward diffusion process progressively turns the data \mathbf{x}_0 into pure noise \mathbf{x}_T through a series of steps, which is defined as:

$$q(\mathbf{x}_t | \mathbf{x}_{t-1}) = \mathcal{N}(\mathbf{x}_t; \sqrt{1 - \beta_t} \mathbf{x}_{t-1}, \beta_t \mathbf{I}), \quad (1)$$

where β_t is a scheduling parameter controlling the noise level at each step, and t denotes the time step.

After T steps, the distribution converges to a standard normal form as: $\mathbf{x}_T \sim \mathcal{N}(0, \mathbf{I})$. The reversed diffusion process reconstructs the original data distribution by learning a denoising model $p_{\theta}(\mathbf{x}_{t-1} | \mathbf{x}_t)$ as follows:

$$p_{\theta}(\mathbf{x}_{t-1} | \mathbf{x}_t) = \mathcal{N}(\mathbf{x}_{t-1}; \mu_{\theta}(\mathbf{x}_t, t), \sigma^2(t) \mathbf{I}), \quad (2)$$

where μ_{θ} represents the denoising mean learned by a neural network to approximate the original data distribution, and $\sigma^2(t)$ denotes the noise variance at step t . By repeatedly applying this denoising step, the model progressively refines the noisy inputs, ultimately generating high-quality samples from an initial random noise distribution.

Model Quantization. Model quantization [17] reduces memory and computational costs by converting model parameters and activations into lower-bit integers. This process utilizes a scale s and zero-point bias z to compensate for data distribution shifts. For a floating-point vector \mathbf{x} , the quantization and dequantization operations are defined as:

$$\begin{cases} x_{\text{int}} = \text{CLIP}\left(\frac{\mathbf{x}-z}{s}, l, u\right) \\ \hat{\mathbf{x}} = s \cdot x_{\text{int}} + z \end{cases}, \quad (3)$$

where x_{int} refers to the quantized integer form and $\hat{\mathbf{x}}$ is simulated quantized form. s controls quantization precision, and z adjusts the data offset before scaling. $\text{CLIP}(\cdot, l, u)$ ensures values remain within the specified range $[l, u]$.

Due to the non-differentiability of rounding in quantization, we utilize the straight-through estimator (STE [30]) to approximate gradients for the quantization training:

$$\frac{\partial L(x)}{\partial x} \approx \begin{cases} 1 & \text{if } x \in [l, u] \\ 0 & \text{otherwise.} \end{cases}, \quad (4)$$

Equivalent Transformation. Outliers in weight and activation distribution have negative effects on quantization, decreasing the quantized model performance largely. For a linear layer with weight W , activation X and bias B , we can conduct equivalent transformation with scale ϕ and offset γ to change quantizers' target to \tilde{W} and \tilde{X} as [60]:

$$\tilde{X} = (X - \delta) \oslash \phi, \tilde{W} = \phi \odot W, \tilde{B} = B + \gamma W, \quad (5)$$

where \odot , \oslash are element-wise multiplication and division. ET adjusts weight and activation distribution and is an effective method to eliminate outliers for quantization [32].

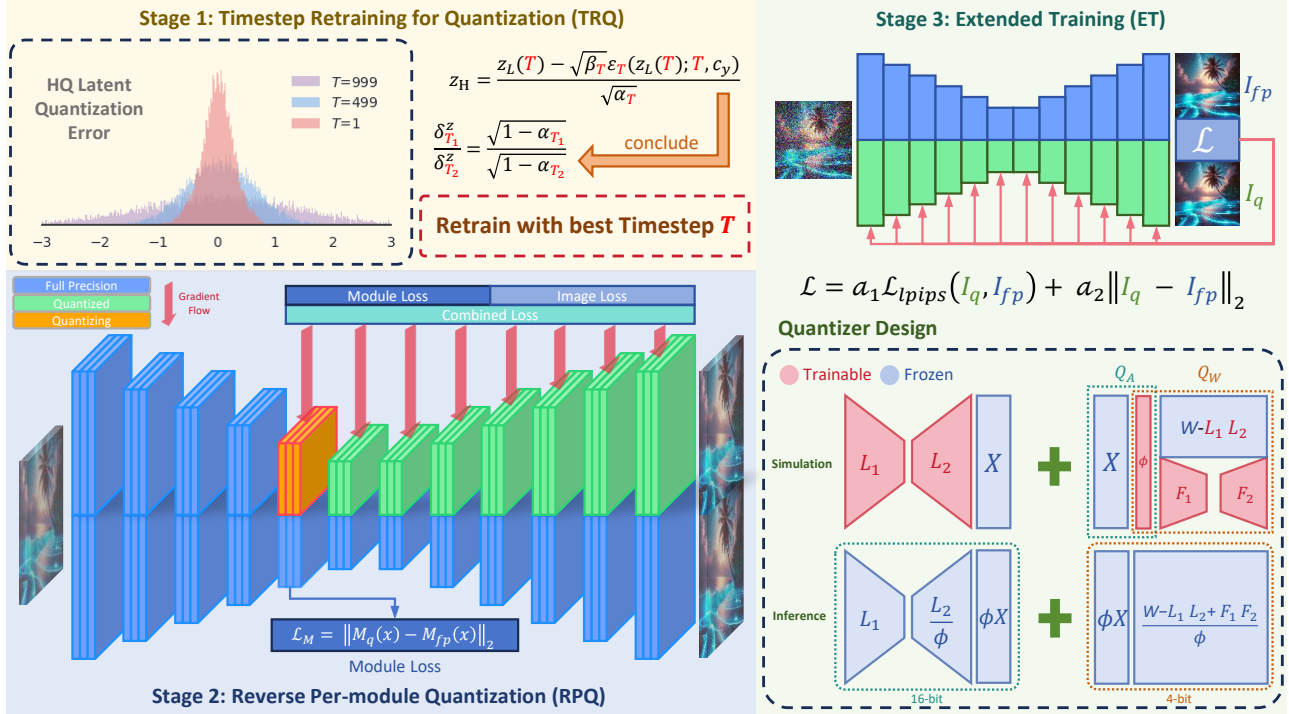


Figure 4. Overview of our QArtSR. Stage 1: we research the relationship between timestep and quantization error. We retrain the OSDSR with the best timestep T before quantization. Stage 2: we propose a reversed per-module quantization strategy to make the process of quantization finetuning more smooth. Stage 3: we need to carry on the extended end-to-end training to enhance the performance further.

3.2. Timestep Retraining for Quantization (TRQ)

As mentioned in OSEDiff [47], the LR-to-HR latent transformation is commonly used in one-step diffusion-based image super-resolution (OSDSR) models, connecting the UNet and VAE decoder. It has a great impact on model quantization due to the selection of timesteps.

The LR-to-HR latent transformation F_T is formulated as a text-conditioned image-to-image denoising process in Eq. (6). Utilizing the predicting noise function ϵ_T of Unet, it conducts only one-step denoising on the LR latent Z_L to obtain the HR latent Z_H at the T -th diffusion timestep.

$$Z_H = F_T(Z_L; c_y) = \frac{Z_L - \sqrt{\beta_T} \epsilon_T(Z_L; T, c_y)}{\sqrt{\alpha_T}}, \quad (6)$$

where α_T and β_T are the scalars that are dependent to the timestep T and they satisfy the condition, $\beta_T = 1 - \alpha_T$. To demonstrate the influence of timestep T on the quantization error, we introduce the theorem below.

Theorem: The high-resolution (HR) latent Z_H 's quantization error $\delta^Z(T)$ is proportional to $\lambda = \sqrt{1 - \alpha_T}$.

$$\delta^Z(T) \propto \lambda = \sqrt{1 - \alpha_T}. \quad (7)$$

We provide the detailed proof for this theorem in the supplementary material. We display value of α and λ as timestep T varies in Fig. 5. Timestep T selection plays a crucial role in reducing HR latent quantization error and improving the HR image quality. It is obvious that $T = 1,000$, which OSEDiff takes, leads to the largest quantization error while $T = 1$ leads to the smallest quantization error.

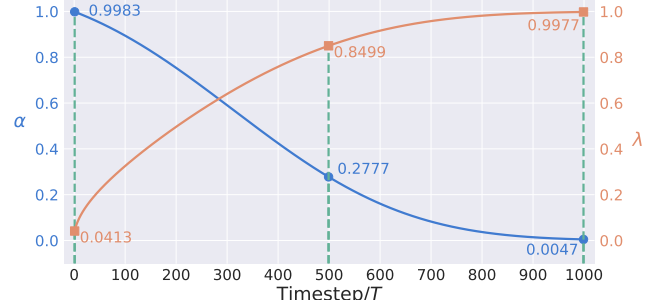


Figure 5. The value of α and λ of different timestep T .

To prove our theorem, we also provide the experimental results of different timesteps (1,000, 500, and 1) models under different bits settings (W32A32, W8A8, W4A4, and W2A2) in Tab. 1. The model performances of different timesteps are evenly matched under the full-precision setting. The model of the smaller timestep tends to demonstrate stronger performance as the bits number decreases.

It is worth noting that the timestep T has nothing to do with the number of denoising steps of diffusion-based models. We only concentrate on how the value of timestep T impacts quantization while there is still only one denoising step in our full-precision backbone model.

In order to minimize the quantization error, we select $T = 1$ as the best timestep and retrain the model with the best timestep as our full-precision backbone. This retrained model with $T = 1$ provides a strong foundation for further quantization experiments and applications.

| Datasets | Bits | Timestep T | PSNR \uparrow | SSIM \uparrow | LPIPS \downarrow | DISTS \downarrow | NIQE \downarrow | MUSIQ \uparrow | MANIQA \uparrow | CLIP-IQA \uparrow |
|----------|--------|--------------|-----------------|-----------------|--------------------|--------------------|-------------------|------------------|-------------------|---------------------|
| RealSR | W32A32 | 1,000 | 25.27 | 0.7379 | 0.3027 | 0.1808 | 4.355 | 67.43 | 0.4766 | 0.6835 |
| | | 500 | 26.11 | 0.7442 | 0.2898 | 0.1820 | 4.414 | 67.73 | 0.4551 | 0.6939 |
| | | 1 | 25.39 | 0.7195 | 0.3251 | 0.1918 | 4.246 | 67.59 | 0.4649 | 0.6859 |
| | W8A8 | 1,000 | 25.26 | 0.7298 | 0.3202 | 0.1862 | 4.334 | 66.82 | 0.464 | 0.6854 |
| | | 500 | 26.15 | 0.7444 | 0.2929 | 0.1835 | 4.406 | 67.43 | 0.4526 | 0.6916 |
| | | 1 | 26.03 | 0.7499 | 0.2806 | 0.1726 | 4.234 | 66.93 | 0.4458 | 0.6707 |
| | W4A4 | 1,000 | 16.01 | 0.5033 | 0.7016 | 0.3668 | 5.520 | 31.26 | 0.2771 | 0.3099 |
| | | 500 | 24.16 | 0.6415 | 0.5963 | 0.386 | 6.855 | 35.47 | 0.2411 | 0.3069 |
| | | 1 | 26.31 | 0.7328 | 0.4423 | 0.3035 | 7.280 | 38.49 | 0.2010 | 0.3941 |
| | W2A2 | 1,000 | 14.88 | 0.2181 | 0.7263 | 0.4584 | 8.525 | 33.12 | 0.2187 | 0.2190 |
| | | 500 | 21.02 | 0.6398 | 0.4586 | 0.2849 | 8.292 | 36.96 | 0.2382 | 0.2255 |
| | | 1 | 26.01 | 0.7453 | 0.4462 | 0.2741 | 7.455 | 37.46 | 0.1826 | 0.2932 |

Table 1. MaxMin quantization experiments ($\times 4$) of OSEDiff [47] on RealSR [18] under different timestep T and bits settings. $WwAa$ denotes w bits weight and a bits activation quantization. The best results in the same setting are colored with red.

3.3. Reversed Per-module Quantization (RPQ)

In the ultra-low-bit settings, quantizing all modules leads to significant performance degradations, and end-to-end training struggles to recover the model’s performance. Providing a better starting point for finetuning allows faster convergence with the reduced time and GPU resource consumption. Inspired by EfficientQAT [4], we propose a reversed per-module quantization strategy by reversing quantization order compared to the forward inference sequence.

Original per-module quantization finetuning focuses on partial optimization, often neglecting overall performance. Even if each quantized module achieves minimal error, the overall image quality may not be optimal. Therefore, we also need to concentrate on the quality of the final quantized image while training certain quantized modules.

The image and module losses are designed as follows:

$$\begin{cases} L_{\text{image}} = a_1 L_{\text{lips}}(I_q, I_{fp}) + a_2 \|I_q - I_{fp}\|_2, \\ L_M = \|M_q(x) - M_{fp}(x)\|_2 \end{cases}, \quad (8)$$

where I_q , I_{fp} indicate the quantized, full-precision image and M_q , M_{fp} indicate the quantized, full-precision module. $\|\cdot\|_2$ indicates the mean square error (MSE) loss. L_{lips} refers to the reference-based evaluation metrics LPIPS [56]. a_1 and a_2 are weighting factors of the two losses.

To consider module and image losses simultaneously, we reverse the forward inference module sequence as the per-module quantization order. Starting from the module closest to output obtains more faithful quantized images, which reflects the current quantized model’s performance better. If the quantization order is the same as the inference sequence, there are plenty of FP modules behind the quantized modules. They may recover the performance of quantized modules to some extent, so that the quantized image may not align with the performance of the model.

The introduction of a new quantized module requires the previously quantized modules to be updated simultaneously to achieve the optimal final quantized image. After the last module is quantized and introduced to the model, RPQ is transformed into end-to-end training eventually.

| Method | Bits | Params / M (\downarrow Ratio) | Ops / G (\downarrow Ratio) |
|--------------|--------|----------------------------------|-------------------------------|
| OSEDiff [47] | W32A32 | 1,303 ($\downarrow 0\%$) | 4,523 ($\downarrow 0\%$) |
| QArtSR | W4A4 | 122 ($\downarrow 90.66\%$) | 531 ($\downarrow 88.26\%$) |
| | W3A3 | 92 ($\downarrow 92.94\%$) | 398 ($\downarrow 91.19\%$) |
| | W2A2 | 62 ($\downarrow 95.21\%$) | 266 ($\downarrow 94.12\%$) |

Table 2. Params, Ops, and compression ratio of different quantization settings. Ops are computed with output size 512×512 .

RPQ’s main disadvantage is that the later quantized modules receive fewer updates than earlier ones, resulting in insufficient training and potential performance degradation. Therefore, extended training (ET) is essential to ensure all modules are finetuned fully for better performance.

3.4. Finetuning Quantizer Design of QArtSR

Inspired by recent quantization works [14, 23, 32, 36], we propose a specialized finetuning quantizer that minimizes the quantization error while adding minimal storage and computational overhead. This approach effectively balances the model performance and efficiency, making it highly suitable for resource-constrained environments.

For a linear layer with weight W , bias B , and activation x , we can design the finetuning quantizer as follows:

$$\begin{aligned} y_q &= Q_W(W)Q_A(x) + Q_B(B) \\ &= L_1 L_2 x + Q_W(\phi(R + F_1 F_2))Q_A\left(\frac{x}{\phi}\right) + Q_B(B), \end{aligned} \quad (9)$$

where $R = W - L_1 L_2$. Q_W , Q_B , and Q_A refer to the weight, bias, and activation quantizer. L and F are low-rank matrices. ϕ is the scale of equivalent transformation.

In this quantizer, ϕ , L , and F are trainable parameters to improve the quantized layer’s performance. L serves as a low-cost full-precision skip connection between the input and quantized output. F finetunes the residual matrix R , while ϕ can mitigate outliers and balance quantization pressure between the weights and activations.

During the finetuning process of RPQ, only quantization and finetuning parameters are updated, while the original model weights are frozen. The scale of trainable parameters is much smaller than that of model’s weights, resulting in a relatively low finetuning cost of memory and time.

| Datasets | Bits | Methods | PSNR↑ | SSIM↑ | LPIPS↓ | DISTS↓ | NIQE↓ | MUSIQ↑ | MANIQA↑ | CLIP-IQA↑ |
|---------------|--------|------------------|-------|--------|--------|--------|--------|--------|---------|-----------|
| RealSR [18] | W32A32 | OSEDiff [47] | 25.27 | 0.7379 | 0.3027 | 0.1808 | 4.355 | 67.43 | 0.4766 | 0.6835 |
| | | MaxMin [17] | 16.01 | 0.5033 | 0.7016 | 0.3668 | 5.520 | 31.26 | 0.2771 | 0.3099 |
| | | LSQ [2] | 21.16 | 0.6703 | 0.4895 | 0.2964 | 8.906 | 42.43 | 0.2332 | 0.2526 |
| | | Q-DM [27] | 19.27 | 0.5711 | 0.4678 | 0.3268 | 5.387 | 48.04 | 0.2560 | 0.4706 |
| | | EfficientDM [14] | 10.70 | 0.5027 | 0.8609 | 0.3974 | 5.846 | 30.21 | 0.2016 | 0.2141 |
| | | PassionSR [60] | 22.52 | 0.6255 | 0.4913 | 0.3185 | 5.706 | 43.21 | 0.2396 | 0.3089 |
| | W4A4 | SVDQuant [23] | 25.98 | 0.7271 | 0.4618 | 0.2665 | 5.645 | 42.84 | 0.2555 | 0.3986 |
| | | QArtSR (ours) | 24.50 | 0.7092 | 0.3761 | 0.2221 | 4.808 | 64.87 | 0.4656 | 0.6999 |
| | | MaxMin [17] | 14.88 | 0.2181 | 0.7263 | 0.4584 | 8.525 | 33.12 | 0.2187 | 0.2190 |
| | | LSQ [2] | 9.16 | 0.0839 | 0.8191 | 0.5401 | 15.48 | 34.55 | 0.3001 | 0.2997 |
| | | Q-DM [27] | 21.44 | 0.6215 | 0.6229 | 0.3063 | 9.081 | 40.37 | 0.2338 | 0.2959 |
| | | EfficientDM [14] | 11.81 | 0.4496 | 0.6879 | 0.3684 | 8.300 | 35.38 | 0.2453 | 0.3464 |
| Urban100 [15] | W2A2 | PassionSR [60] | 14.56 | 0.2330 | 0.7609 | 0.4904 | 8.356 | 37.54 | 0.2376 | 0.3694 |
| | | SVDQuant [23] | 18.41 | 0.5941 | 0.4921 | 0.3265 | 5.953 | 42.82 | 0.2447 | 0.3659 |
| | | QArtSR (ours) | 24.92 | 0.6353 | 0.5825 | 0.2983 | 5.942 | 40.98 | 0.3102 | 0.4865 |
| | | MaxMin [17] | 21.55 | 0.6511 | 0.2122 | 0.1461 | 4.622 | 72.48 | 0.4933 | 0.6628 |
| | | LSQ [2] | 12.01 | 0.1372 | 0.7975 | 0.4549 | 5.674 | 47.77 | 0.2671 | 0.2343 |
| | | Q-DM [27] | 18.19 | 0.5616 | 0.5172 | 0.3366 | 8.490 | 50.80 | 0.2793 | 0.2747 |
| | W32A32 | EfficientDM [14] | 17.64 | 0.5207 | 0.4975 | 0.3336 | 5.052 | 51.50 | 0.2932 | 0.4213 |
| | | PassionSR [60] | 10.90 | 0.4528 | 0.7672 | 0.3958 | 5.400 | 38.17 | 0.2303 | 0.2327 |
| | | SVDQuant [23] | 19.20 | 0.5325 | 0.5680 | 0.3440 | 6.131 | 46.99 | 0.2617 | 0.3083 |
| | | QArtSR (ours) | 22.30 | 0.6113 | 0.3764 | 0.2493 | 4.708 | 55.98 | 0.3415 | 0.4339 |
| | | MaxMin [17] | 22.18 | 0.6377 | 0.2507 | 0.1712 | 4.227 | 69.82 | 0.4514 | 0.6451 |
| | | LSQ [2] | 12.76 | 0.3171 | 0.8899 | 0.4525 | 9.417 | 33.75 | 0.2987 | 0.2674 |
| DIV2K_val [1] | W4A4 | Q-DM [27] | 8.39 | 0.0797 | 0.8500 | 0.5337 | 15.491 | 44.37 | 0.3031 | 0.2918 |
| | | EfficientDM [14] | 18.34 | 0.5802 | 0.5559 | 0.3448 | 8.634 | 48.88 | 0.2791 | 0.3157 |
| | | PassionSR [60] | 11.69 | 0.4116 | 0.7075 | 0.3910 | 8.348 | 42.06 | 0.2672 | 0.3479 |
| | | SVDQuant [23] | 12.35 | 0.1727 | 0.8462 | 0.4953 | 9.636 | 47.15 | 0.3272 | 0.3491 |
| | | QArtSR (ours) | 17.40 | 0.5687 | 0.4767 | 0.3102 | 6.063 | 50.06 | 0.3001 | 0.3981 |
| | | MaxMin [17] | 21.96 | 0.5682 | 0.4299 | 0.2720 | 4.508 | 55.48 | 0.3878 | 0.5229 |
| | W2A2 | LSQ [2] | 14.50 | 0.2320 | 0.8159 | 0.3660 | 8.609 | 33.22 | 0.2374 | 0.2781 |
| | | Q-DM [27] | 9.11 | 0.1083 | 0.8709 | 0.5272 | 13.73 | 44.51 | 0.3074 | 0.3614 |
| | | EfficientDM [14] | 20.03 | 0.5681 | 0.5858 | 0.3274 | 8.105 | 42.63 | 0.2342 | 0.3727 |
| | | PassionSR [60] | 12.10 | 0.4674 | 0.7471 | 0.3599 | 7.936 | 35.80 | 0.2525 | 0.3799 |
| | | SVDQuant [23] | 13.57 | 0.2195 | 0.8486 | 0.4940 | 8.526 | 46.53 | 0.3325 | 0.4326 |
| | | QArtSR (ours) | 18.99 | 0.6348 | 0.4947 | 0.2716 | 5.623 | 43.83 | 0.2409 | 0.3575 |

Table 3. Quantitative quantization experiments ($\times 4$) results. The full-precision backbone is OSEDiff [47] ($T=1,000$). The best and second best results in the same setting are colored with red and blue. $WwAa$ denotes w bits weight and a bits activation quantization.

4. Experiments

4.1. Experiment Setup

Data Construction. We randomly extract 512 pairs of low-resolution (LR) and high-resolution (HR) images, each with a dimension of 128×128 , from the DIV2K_train dataset [1] to build the calibration set. For testing, we use datasets including RealSR [18], Urban100 [15], and DIV2K_val [1].

Evaluation Metrics. We adopt reference-based evaluation metrics such as PSNR, SSIM [45], LPIPS [56], and DISTS [8]. Additionally, we apply non-reference metrics, like NIQE [55], MUSIQ [19], MANIQA [49], and CLIP-IQA [41]. All methods are evaluated using full-size images.

Implementation Details. Learning rate for QArtSR is set to 1×10^{-5} . Experiments are conducted on RTX A6000, consuming 36.8 GB GPU memory and 6.8 hours GPU time, which are close to advanced PTQ methods [14, 23].

Compared Methods. We compare QArtSR with several representative quantization methods: MaxMin [17], LSQ [12], Q-DM [27], EfficientDM [14], PassionSR [60], and SVDQuant [23]. We adopt these quantization methods on OSEDiff [47] based on their released code. Q-DM, EfficientDM, and SVDQuant are newly proposed quantization methods for multi-step diffusion models.

Compression Ratio. We calculate the total model size (Params / M) and the number of operations (Ops / G), following the methodology adopted in prior quantization studies [33]. The results, summarized in Tab. 2, present the compression and acceleration ratios for the various settings with scaling factor 4. In 4-bit configuration, QArtSR achieves a compression ratio of 90.66% and an acceleration ratio of 88.26%, while those in 2-bit setting are 95.21% and 94.12%, compared to the FP OSEDiff model.

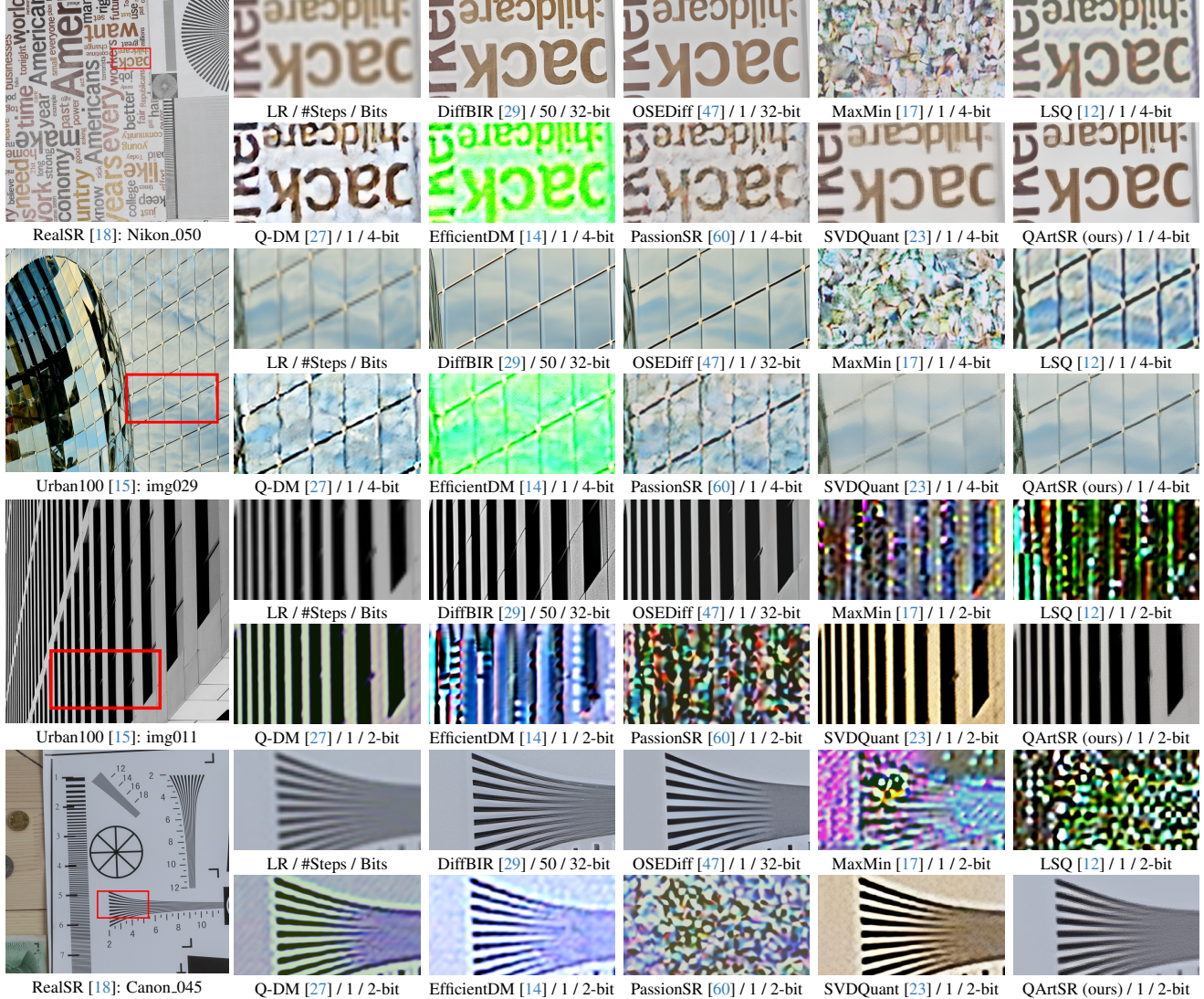


Figure 6. Visual comparison ($\times 4$) of high-resolution images, full-precision model outputs, and various quantization methods in challenging cases under W4A4 and W2A2 settings. QArtSR demonstrates notable visual superiority over other approaches.

| Bits | TRQ | RPQ | | ET | RealSR [18] | | | | | | | |
|------|-----|------|----|----|-----------------------|-------------------------|-------------------------|--------------------|-----------------------|------------------|-------------------|---------------------|
| | | RPQ* | ET | | PSNR \uparrow | SSIM \uparrow | LPIPS \downarrow | DISTS \downarrow | NIQE \downarrow | MUSIQ \uparrow | MANIQA \uparrow | CLIP-IQA \uparrow |
| W4A4 | ✓ | ✓ | ✓ | | 16.01 26.31 | 0.5033 0.7328 | 0.7016 0.4423 | 0.3668 0.3035 | 5.520 7.280 | 31.26 38.49 | 0.2771 0.2010 | 0.3099 0.3941 |
| | ✓ | | ✓ | | 22.36 25.17 | 0.6735 0.7171 | 0.5248 0.4035 | 0.3489 0.2498 | 5.879 5.105 | 47.57 54.93 | 0.2962 0.3584 | 0.5601 0.6184 |
| | ✓ | ✓ | ✓ | | 24.79 | 0.7083 | 0.4113 | 0.2447 | 5.130 | 59.83 | 0.4303 | 0.6516 |
| | ✓ | | | | 24.50 | 0.7092 | 0.3761 | 0.2221 | 4.808 | 64.87 | 0.4656 | 0.6999 |

Table 4. Ablation study ($\times 4$) on the key components of our proposed method: TRQ and RPQ. RPQ consists of two stages: per-module quantization training (RPQ*) and extended training (ET). The best and second-best results in this setting are highlighted in red and blue.

4.2. Main Results

Quantitative Results. Table 3 presents the quantitative results of 4-bit and 2-bit settings. QArtSR significantly outperforms other quantization methods in both settings. In 4-bit setting, QArtSR performs comparably with the FP model and even surpasses it in certain metrics. While QArtSR is outperformed by SVDQuant [23] in some met-

rics, such as PSNR and SSIM, QArtSR maintains a significant advantage across a broader range of evaluation criteria. Other 4-bit models show a large performance gap compared to the FP model, highlighting QArtSR’s effectiveness. In 2-bit setting, other models suffer severe performance drops, while QArtSR achieves the smallest performance gap and proves its robustness in ultra-low-bit quantization.

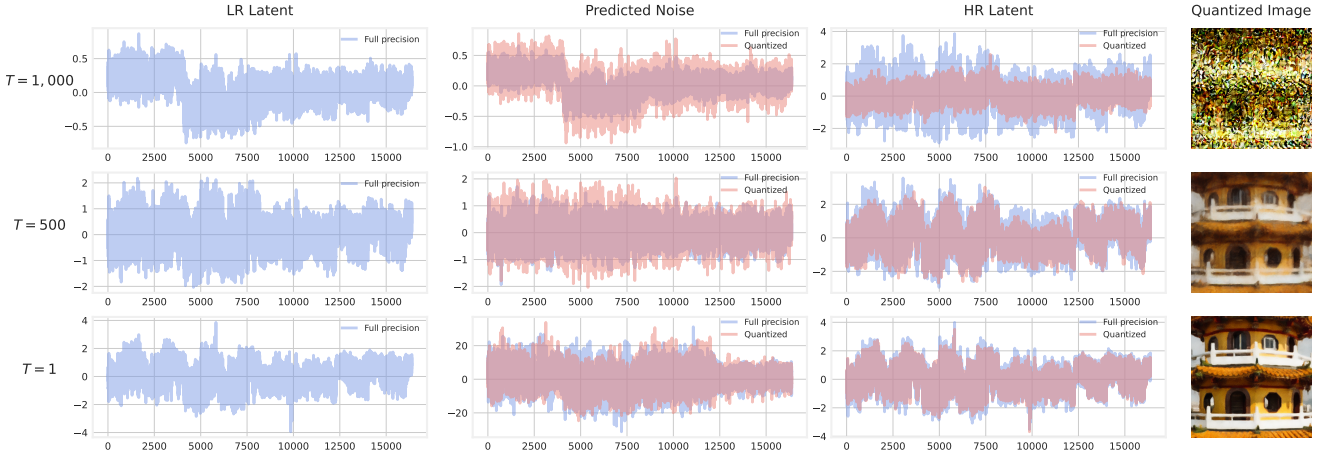


Figure 7. Visualization of three essential staged outputs and the quantized image in OSEDiff [47] under $T=1,000, 500, 1$ respectively.

Visual Comparison. Figure 6 shows a visual comparison ($\times 4$), highlighting many challenging cases for better and clearer contrast. QArtSR produces sharper details and more refined textures than other comparison methods. There is a minor gap between the 4-bit QArtSR and the full-precision model, indicating QArtSR’s outstanding performance. Compared with 4-bit quantized models, the performance distinction among the 2-bit quantization methods is more pronounced. Although the 2-bit QArtSR exhibits obvious performance degradation, it outperforms other comparison methods by a large margin. It still retains much expression ability for clearer HR images while the other 2-bit quantized models almost fail to generate HR images.

4.3. Feature Visualization

In Fig. 7, we present three key staged features along with the corresponding quantized images for $T=1,000, 500, 1$, respectively. Aiming at illustrating the effects of model quantization in Eq. (6), we utilize the output from the full-precision VAE encoder as LR latent, providing a clear reference for comparison between FP and quantized models. It is evident that the quantization error of the predicted noise is the largest when $T=1$ while the quantization errors of the HR latent and the quantized image are the smallest instead. This consistency between experimental results and our theory further reinforces the validity of our approach.

4.4. Ablation Study

Timestep Retraining for Quantization (TRQ). The results presented in Tab. 1 indicate that the quantized model under timestep $T = 1$ achieves superior performance, especially at ultra-low-bit settings. It highlights the effectiveness of retraining the backbone model with better timestep for quantization. The improvements are especially noticeable for aggressive quantization, confirming that the choice of timestep plays a crucial role in preserving model performance. Ablation study results in Tab. 4 also demonstrate that the introduction of TRQ brings great enhancement to the baseline and RPQ* on most of the evaluation metrics.

Reversed Per-module Quantization (RPQ*). To evaluate the effects of RPQ*, we conduct two comparative experiments, as shown in Tab. 4. RPQ* significantly outperforms the baseline, showing substantial improvements across most of the evaluation metrics. Furthermore, when RPQ* is integrated into the TRQ framework, it contributes to notable gains in performance on nearly all metrics, highlighting its effectiveness in enhancing the overall model performance.

Extended Training (ET). As shown in Tab. 4, comparing TRQ and TRQ+ET reveals that the incorporation of extended training significantly enhances the performance of the quantized model. Furthermore, by combining ET with TRQ+RPQ*, which involves extending the training epochs after RPQ*, we observe a substantial improvement in the model’s performance. The extended training enables the quantized model to recover more effectively from the performance degradation caused by quantization, leading to a more robust and efficient quantized model.

5. Conclusion

We propose QArtSR, a novel quantization method for one-step diffusion-based image SR models. First, we investigate impact of timestep values on OSDSR quantization. We propose the timestep retraining quantization (TRQ) strategy, easing subsequent quantization and enabling high performance even under ultra-low-bit settings. Additionally, we propose a reversed per-module quantization (RPQ) technique relative to the inference sequence, allowing joint optimization of module and image loss. We then apply extended training after per-module stage to ensure that quantized modules are fully finetuned. Quantization experiments demonstrate that QArtSR delivers perceptual quality compared with FP models at 4-bit and preserves most of its performance even at 2-bit. It surpasses recent diffusion quantization methods, establishing itself as a strong candidate for OSDSR quantization. This work lays the foundation for the future advancements in OSDSR quantization and the practical deployment of high-performance SR models.

References

[1] Eirikur Agustsson and Radu Timofte. Ntire 2017 challenge on single image super-resolution: Dataset and study. In *CVPRW*, 2017. 6

[2] Yash Bhalgat, Jinwon Lee, Markus Nagel, Tijmen Blankevoort, and Nojun Kwak. Lsq+: Improving low-bit quantization through learnable offsets and better initialization. In *CVPR*, 2020. 2, 3, 6

[3] Yelysei Bondarenko, Riccardo Del Chiaro, and Markus Nagel. Low-rank quantization-aware training for llms. *arXiv preprint arXiv:2406.06385*, 2024. 3

[4] Mengzhao Chen, Wenqi Shao, Peng Xu, Jiahao Wang, Peng Gao, Kaipeng Zhang, Yu Qiao, and Ping Luo. Efficientqat: Efficient quantization-aware training for large language models. *arXiv preprint arXiv:2407.11062*, 2024. 3, 5

[5] Zheng Chen, Yulun Zhang, Jinjin Gu, Linghe Kong, Xin Yuan, et al. Cross aggregation transformer for image restoration. In *NeurIPS*, 2022. 1

[6] Zheng Chen, Yulun Zhang, Jinjin Gu, Linghe Kong, Xin Yuan, et al. Cross aggregation transformer for image restoration. In *NeurIPS*, 2022. 3

[7] Zheng Chen, Yulun Zhang, Jinjin Gu, Linghe Kong, Xiaokang Yang, and Fisher Yu. Dual aggregation transformer for image super-resolution. In *ICCV*, 2023. 1

[8] Keyan Ding, Kede Ma, Shiqi Wang, and Eero P Simoncelli. Image quality assessment: Unifying structure and texture similarity. In *TPAMI*, 2020. 6

[9] Yifu Ding, Haotong Qin, Qinghua Yan, Zhenhua Chai, Junjie Liu, Xiaolin Wei, and Xianglong Liu. Towards accurate post-training quantization for vision transformer. In *ACM MM*, 2022. 1

[10] Chao Dong, Chen Change Loy, Kaiming He, and Xiaoou Tang. Image super-resolution using deep convolutional networks. In *TPAMI*, 2015. 1

[11] Dayou Du, Yijia Zhang, Shijie Cao, Jiaqi Guo, Ting Cao, Xiaowen Chu, and Ningyi Xu. Bitdistiller: Unleashing the potential of sub-4-bit llms via self-distillation. In *ACL*, 2024. 3

[12] Steven K Esser, Jeffrey L McKinstry, Deepika Bablani, Rathinakumar Appuswamy, and Dharmendra S Modha. Learned step size quantization. In *ICLR*, 2020. 6, 7

[13] Yefei He, Luping Liu, Jing Liu, Weijia Wu, Hong Zhou, and Bohan Zhuang. Ptqd: Accurate post-training quantization for diffusion models. In *NeurIPS*, 2023. 3

[14] Yefei He, Jing Liu, Weijia Wu, Hong Zhou, and Bohan Zhuang. Efficientdm: Efficient quantization-aware fine-tuning of low-bit diffusion models. In *ICLR*, 2024. 2, 3, 5, 6, 7

[15] Jia-Bin Huang, Abhishek Singh, and Narendra Ahuja. Single image super-resolution from transformed self-exemplars. In *CVPR*, 2015. 2, 6, 7

[16] Itay Hubara, Yury Nahshan, Yair Hanani, Ron Banner, and Daniel Soudry. Accurate post training quantization with small calibration sets. In *ICML*, 2021. 1

[17] Benoit Jacob, Skirmantas Kligys, Bo Chen, Menglong Zhu, Matthew Tang, Andrew Howard, Hartwig Adam, and Dmitry Kalenichenko. Quantization and training of neural networks for efficient integer-arithmetic-only inference. In *CVPR*, 2018. 2, 3, 6, 7

[18] Xiaozhong Ji, Yun Cao, Ying Tai, Chengjie Wang, Jilin Li, and Feiyue Huang. Real-world super-resolution via kernel estimation and noise injection. In *CVPRW*, 2020. 5, 6, 7

[19] Junjie Ke, Qifei Wang, Yilin Wang, Peyman Milanfar, and Feng Yang. Musiq: Multi-scale image quality transformer. In *ICCV*, 2021. 6

[20] Jiwon Kim, Jung Kwon Lee, and Kyoung Mu Lee. Accurate image super-resolution using very deep convolutional networks. In *CVPR*, 2016. 3

[21] Eli Kravchik, Fan Yang, Pavel Kisilev, and Yoni Choukroun. Low-bit quantization of neural networks for efficient inference. In *ICCVW*, 2019. 1

[22] Jianze Li, Jiezhang Cao, Zichen Zou, Xiongfei Su, Xin Yuan, Yulun Zhang, Yong Guo, and Xiaokang Yang. Distillation-free one-step diffusion for real-world image super-resolution. *arXiv preprint arXiv:2410.04224*, 2024. 1

[23] Muyang Li, Yujun Lin, Zhekai Zhang, Tianle Cai, Xiuyu Li, Junxian Guo, Enze Xie, Chenlin Meng, Jun-Yan Zhu, and Song Han. Svdqunat: Absorbing outliers by low-rank components for 4-bit diffusion models. In *ICLR*, 2025. 2, 3, 5, 6, 7

[24] Xiuyu Li, Yijiang Liu, Long Lian, Huanrui Yang, Zhen Dong, Daniel Kang, Shanghang Zhang, and Kurt Keutzer. Q-diffusion: Quantizing diffusion models. In *ICCV*, 2023. 3

[25] Yuhang Li, Ruihao Gong, Xu Tan, Yang Yang, Peng Hu, Qi Zhang, Fengwei Yu, Wei Wang, and Shi Gu. Brecq: Pushing the limit of post-training quantization by block reconstruction. In *ICLR*, 2021. 3

[26] Yixiao Li, Yifan Yu, Chen Liang, Pengcheng He, Nikos Karampatziakis, Weizhu Chen, and Tuo Zhao. Loftq: Lora-fine-tuning-aware quantization for large language models. In *ICLR*, 2023. 3

[27] Yanjing Li, Sheng Xu, Xianbin Cao, Xiao Sun, and Baochang Zhang. Q-dm: An efficient low-bit quantized diffusion model. In *NeurIPS*, 2024. 2, 3, 6, 7

[28] Jingyun Liang, Jiezhang Cao, Guolei Sun, Kai Zhang, Luc Van Gool, and Radu Timofte. Swinir: Image restoration using swin transformer. In *ICCV*, 2021. 1, 3

[29] Xinqi Lin, Jingwen He, Ziyan Chen, Zhaoyang Lyu, Bo Dai, Fanghua Yu, Wanli Ouyang, Yu Qiao, and Chao Dong. Diffbir: Towards blind image restoration with generative diffusion prior. In *ECCV*, 2024. 1, 3, 7

[30] Zechun Liu, Kwang-Ting Cheng, Dong Huang, Eric Xing, and Zhiqiang Shen. Nonuniform-to-uniform quantization: Towards accurate quantization via generalized straight-through estimation. In *CVPR*, 2022. 3

[31] Zechun Liu, Barlas Onguz, Changsheng Zhao, Ernie Chang, Pierre Stock, Yashar Mehdad, Yangyang Shi, Raghuraman Krishnamoorthi, and Vikas Chandra. Llm-qat: Data-free quantization aware training for large language models. In *ACL*, 2024. 3

[32] Jiayi Pan, Chengcan Wang, Kaifu Zheng, Yangguang Li, Zhenyu Wang, and Bin Feng. Smoothquant+: Accurate and efficient 4-bit post-training weightquantization for llm. In *ICML*, 2023. 3, 5

[33] Haotong Qin, Yulun Zhang, Yifu Ding, Xianglong Liu, Martin Danelljan, Fisher Yu, et al. Quantsr: accurate low-bit quantization for efficient image super-resolution. In *NeurIPS*, 2023. 6

[34] Robin Rombach, Andreas Blattmann, Dominik Lorenz, Patrick Esser, and Björn Ommer. High-resolution image synthesis with latent diffusion models. In *CVPR*, 2022. 3

[35] Yuzhang Shang, Zhihang Yuan, Bin Xie, Bingzhe Wu, and Yan Yan. Post-training quantization on diffusion models. In *CVPR*, 2023. 3

[36] Wenqi Shao, Mengzhao Chen, Zhaoyang Zhang, Peng Xu, Lirui Zhao, Zhiqian Li, Kaipeng Zhang, Peng Gao, Yu Qiao, and Ping Luo. Omnipquant: Omnidirectionally calibrated quantization for large language models. In *ICLR*, 2024. 3, 5

[37] Jiaming Song, Chenlin Meng, and Stefano Ermon. Denoising diffusion implicit models. In *ICLR*, 2021. 1

[38] Yang Song, Prafulla Dhariwal, Mark Chen, and Ilya Sutskever. Consistency models. In *ICML*, 2023. 1

[39] Yang Sui, Yanyu Li, Anil Kag, Yerlan Idelbayev, Junli Cao, Ju Hu, Dhrithiman Sagar, Bo Yuan, Sergey Tulyakov, and Jian Ren. Bitsfusion: 1.99 bits weight quantization of diffusion model. In *NeurIPS*, 2024. 3

[40] Haoxuan Wang, Yuzhang Shang, Zhihang Yuan, Junyi Wu, Junchi Yan, and Yan Yan. Quest: Low-bit diffusion model quantization via efficient selective finetuning. *arXiv preprint arXiv:2402.03666*, 2024. 3

[41] Jianyi Wang, Kelvin CK Chan, and Chen Change Loy. Exploring clip for assessing the look and feel of images. In *AAAI*, 2023. 6

[42] Jianyi Wang, Zongsheng Yue, Shangchen Zhou, Kelvin CK Chan, and Chen Change Loy. Exploiting diffusion prior for real-world image super-resolution. In *IJCV*, 2024. 1

[43] Xintao Wang, Liangbin Xie, Chao Dong, and Ying Shan. Real-esrgan: Training real-world blind super-resolution with pure synthetic data. In *ICCV*, 2021. 1, 3

[44] Yufei Wang, Wenhan Yang, Xinyuan Chen, Yaohui Wang, Lanqing Guo, Lap-Pui Chau, Ziwei Liu, Yu Qiao, Alex C Kot, and Bihan Wen. Sinsr: diffusion-based image super-resolution in a single step. In *CVPR*, 2024. 1, 3

[45] Zhou Wang, Alan C Bovik, Hamid R Sheikh, and Eero P Simoncelli. Image quality assessment: from error visibility to structural similarity. *TIP*, 2004. 6

[46] Zhengyi Wang, Cheng Lu, Yikai Wang, Fan Bao, Chongxuan Li, Hang Su, and Jun Zhu. Prolificdreamer: High-fidelity and diverse text-to-3d generation with variational score distillation. In *NeurIPS*, 2024. 1

[47] Rongyuan Wu, Lingchen Sun, Zhiyuan Ma, and Lei Zhang. One-step effective diffusion network for real-world image super-resolution. In *NeurIPS*, 2024. 1, 2, 3, 4, 5, 6, 7, 8

[48] Rongyuan Wu, Tao Yang, Lingchen Sun, Zhengqiang Zhang, Shuai Li, and Lei Zhang. Seesr: Towards semantics-aware real-world image super-resolution. In *CVPR*, 2024. 1, 3

[49] Sidi Yang, Tianhe Wu, Shuwei Shi, Shanshan Lao, Yuan Gong, Mingdeng Cao, Jiahao Wang, and Yujiu Yang. Maniq: Multi-dimension attention network for no-reference image quality assessment. In *CVPR*, 2022. 6

[50] Zhewei Yao, Reza Yazdani Aminabadi, Minjia Zhang, Xiaoxia Wu, Conglong Li, and Yuxiong He. Zeroquant: Efficient and affordable post-training quantization for large-scale transformers. In *NeurIPS*, 2022. 3

[51] Tianwei Yin, Michaël Gharbi, Richard Zhang, Eli Shechtman, Fredo Durand, William T Freeman, and Taesung Park. One-step diffusion with distribution matching distillation. In *CVPR*, 2024. 1

[52] Chengting Yu, Shu Yang, Fengzhao Zhang, Hanzhi Ma, Aili Wang, and Er-Ping Li. Improving quantization-aware training of low-precision network via block replacement on full-precision counterpart. *arXiv preprint arXiv:2412.15846*, 2024. 3

[53] Zongsheng Yue, Kang Liao, and Chen Change Loy. Arbitrary-steps image super-resolution via diffusion inversion. In *CVPR*, 2025. 3

[54] Kai Zhang, Jingyun Liang, Luc Van Gool, and Radu Timofte. Designing a practical degradation model for deep blind image super-resolution. In *ICCV*, 2021. 1, 3

[55] Lin Zhang, Lei Zhang, and Alan C. Bovik. A feature-enriched completely blind image quality evaluator. *TIP*, 2015. 6

[56] Richard Zhang, Phillip Isola, Alexei A Efros, Eli Shechtman, and Oliver Wang. The unreasonable effectiveness of deep features as a perceptual metric. In *CVPR*, 2018. 5, 6

[57] Yulun Zhang, Kunpeng Li, Kai Li, Lichen Wang, Bineng Zhong, and Yun Fu. Image super-resolution using very deep residual channel attention networks. In *ECCV*, 2018. 3

[58] Yulun Zhang, Yapeng Tian, Yu Kong, Bineng Zhong, and Yun Fu. Residual dense network for image super-resolution. In *CVPR*, 2018. 1

[59] Wenliang Zhao, Lujia Bai, Yongming Rao, Jie Zhou, and Jiwen Lu. Unipc: A unified predictor-corrector framework for fast sampling of diffusion models. In *NeurIPS*, 2024. 1

[60] Libo Zhu, Jianze Li, Haotong Qin, Yulun Zhang, Yong Guo, and Xiaokang Yang. Passionsr: Post-training quantization with adaptive scale in one-step diffusion based image super-resolution. In *CVPR*, 2025. 1, 2, 3, 6, 7